

# High-temperature Corrosion Investigation of the Inconel-600 in Molten Sulfate/Vanadate Mixtures Using Electrochemical Techniques

*N. S. Flores García, C. Cuevas Arteaga\**

Centro de Investigación en Ingeniería y Ciencias Aplicadas, Universidad Autónoma del Estado de Morelos. Av. Universidad 101. Col. Chamilpa, 62210. Cuernavaca, Mor., México.

\*E-mail: [ccuevas@uaem.mx](mailto:ccuevas@uaem.mx)

*Received: 16 April 2017 / Accepted: 9 June 2017 / Published: 12 September 2017*

---

In this paper, the results obtained from polarization curves (PC) and Electrochemical Impedance Spectroscopy (EIS) for Inconel-600 exposed in two different compositions of corrosive molten salts are presented. The Inconel-600 samples were exposed to high sulfate (80 mol% Na<sub>2</sub>SO<sub>4</sub>-20 mol% V<sub>2</sub>O<sub>5</sub>) and high vanadium (80 mol% V<sub>2</sub>O<sub>5</sub>-20 mol% Na<sub>2</sub>SO<sub>4</sub>) molten salts at 700 °C during 120 h. Tafel slopes, current densities and corrosion potentials were obtained from polarization curves for both corrosive systems. EIS was used to determine the controlling corrosion mechanism, either charge transfer (activation) or mass diffusion, and the charge transfer resistance R<sub>ct</sub>. Scanning electron microscopy analysis (images and mappings) showed that Inconel-600 exposed to the high sulfate molten salt suffered inter-granular corrosion, which was due to an oxidation process through the grain boundaries, just below the metal-scale interface; whereas exposed to the high vanadium molten salt, Inconel-600 corroded by means of a generalized corrosion process, which was due to the diffusion of sulfur to the surface and inside the alloy. The corrosion mechanisms suffered by the Inconel-600 in both corrosive molten salts were supported by X-ray diffraction analyses of the corrosion products, which showed the presence of chromium, iron and nickel oxides together with some vanadates as secondary compounds.

---

**Keywords:** Superalloy, molten salts, hot corrosion, EIS.

## 1. INTRODUCTION

High temperature corrosion by molten salts, also known as hot corrosion, is a phenomenon observed in power plants using residual fuel oils, in which the metallic surfaces are covered by a thin molten salt layer exposed to a gaseous environment [1]. The corrosion by molten salts has been also

called vanadium attack due to the species vanadium contributes most to the corrosion of metallic alloys at high temperatures [2-3].

Vanadium is chemically very active at 650 °C, producing several complex compounds, which led to a significant vanadium attack of the metal surfaces [4]. This degradation process affects the physical, chemical and mechanical properties of materials [5]. Due to economic reasons, the high-grade oil has a very limited utilization, so that, the residual fuel oil is widely demanded, especially in power plants generation. Fuel oil is the main responsible for producing high temperature corrosion by molten salts. During combustion, the fossil fuels produce compounds with low melting points, presenting high concentrations of vanadium, sodium and sulfur, which form some compounds such as  $\text{Na}_2\text{SO}_4$  and  $\text{V}_2\text{O}_5$ , and some other complex compounds named sodium vanadyl vanadates [2-4]. These compounds are deposited on the surface of metallic components of boilers, gas turbines and furnaces, and when the temperature is above their melting points, they become liquids and may generate a catastrophic corrosion phenomenon [6-8]. Nickel base superalloys are very common commercial materials, fabricated for being used in high temperature atmospheres [9]. Nickel base superalloys are normally used in gas turbines, nuclear power plant reactors, steam turbines, etc. [10]. The chemical composition of nickel base alloys contains nickel from 38% to 76%, up to 27% chromium and 20% cobalt. Some alloys in this group are the Hastelloy, Inconel, Nimonic, Udimet and Waspaloy series [11].

In the present paper, the electrochemical impedance spectroscopy (EIS) technique and potentiodynamic polarization curves (PPC) were used to study the Inconel-600 exposed to molten salts with two different compositions: 80 mol%  $\text{Na}_2\text{SO}_4$  – 20 mol%  $\text{V}_2\text{O}_5$  (high sulfate) and 80 mol%  $\text{V}_2\text{O}_5$  – 20 mol%  $\text{Na}_2\text{SO}_4$  (high vanadium) at 700°C for 120 h. Corrosion behavior was supported by physical characterization of the corroded samples from scanning electron microscopy (SEM) analyses, and chemical characterization of the corrosion products by X-ray diffraction analyses.

## 2. EXPERIMENTAL PROCEDURE

### 2.1. Material.

**Table 1.** Composition of the Inconel-600 (wt. %).

Si	Cu	S	Cr	Mn	Ni	C	Fe
0.50	0.50	0.015	16	1	<b>72</b>	0.015	9

The composition of Inconel-600 is shown in table 1, observing the significant amount of chromium and in a lesser extend of nickel. An Inconel-600 bar was cut as small rectangles parallelepipeds of 10x6x6 mm. Then, the samples were ground to 600 grit silicon carbide paper, washed with distilled water, degreased with ethyl alcohol and dried under a flow of hot air stream.

## 2.2. Working electrodes and reference electrodes preparation.

To achieve an electrical connection, the working electrodes (Inconel-600) were welded to an 80 wt% Cr-20Ni wire (300 mm long, 1.0 mm in diameter). In order to isolate the 80Cr-Ni wire from the molten salt, this was introduced into ceramic tubes. The gap between the ceramic tube and the electrical connection wire was filled with refractory cement.

Two 1 mm diameter/200 mm long of platinum wires were used as reference and auxiliary electrodes, which were washed with ethyl alcohol and dried with hot air. Platinum electrodes have been widely used under similar conditions [12-14]. The platinum wires were also isolated in ceramic tubes and sealed with refractory cement, leaving 5mm of free length for contacting with the molten salts.

## 2.3. Corrosive salts preparation.

Two corrosive salts were utilized in this work: 80 mol%  $\text{Na}_2\text{SO}_4$  - 20 mol%  $\text{V}_2\text{O}_5$  (high sulfate) and 80 mol%  $\text{V}_2\text{O}_5$  - 20 mol%  $\text{Na}_2\text{SO}_4$  (high vanadium). The preparation of the corrosive mixtures was made from analytical grade reagents. Taking into account the initial area of the specimens, an amount of  $2000 \text{ mg/cm}^2$  of the corrosive salts was introduced into a 30 ml silica crucible, allowing a melt depth of about 3 cm. Afterwards, the crucible was placed inside an electrical tubular furnace to reach the test temperature of  $700 \text{ }^\circ\text{C}$ , which was constantly monitored during the tests using a K-type thermocouple and controlled to  $\pm 4 \text{ }^\circ\text{C}$  with respect to the test temperature. The crucible containing the solid corrosive salts was replaced for every new test. It is important to note that in a real high temperature corrosion process, the alloys are in contact to a thin molten salt layer and a corrosive gas environment; while the experimental procedure carried out in this work, the specimens were exposed in a deep melt with static air, therefore, the experimental conditions and corrosion rates obtained are not representative of those present in power generation boilers [15]. However, bulk molten salt tests are considered a viable experimental procedure for the evaluation of corrosion performance of metallic materials. The size and preparation of the samples, as well as the preparation of the corrosive mixtures were the same for all the electrochemical tests.

## 2.4. Electrochemical tests.

The electrochemical cell was a typical three electrodes setup for both techniques: the working electrode and two platinum electrodes, as the reference and the counter electrodes. The potentiodynamic polarization curves were performed at a scan rate of  $1 \text{ mV/s}$ , this scan rate has been also reported in some other works [4,16,17], and polarized from  $-200 \text{ mV}$  to  $1500 \text{ mV}$  with respect to the corrosion potential ( $E_{\text{corr}}$ ). For electrochemical impedance tests, the applied parameters were: a frequency interval from  $0.001 \text{ Hz}$  to  $10 \text{ KHz}$  and an amplitude of input sine-wave voltage of  $10 \text{ mV}$ . For both techniques, an automated potentiostat/Galvanostat (ACM instruments Auto DC) controlled by a personal computer was used. The experimentation was carried out once the value of the free corrosion potential ( $E_{\text{corr}}$ ) was stable, which was achieved in 40 minutes.

### 2.5. Auxiliary techniques.

Scanning electron microscopy (SEM) allowed the identification and distribution of the corrosion products from mapping analysis of the cross section of the metal-scale interface, and the morphology of the cleaned corroded specimens obtained from the tests carried out under the two different corrosive mixtures. In order to determine the type of corrosion suffered by the Inconel-600, images of the most representative morphologies were taken. For obtaining the SEM mappings of the cross section of the metal-scale interface, the corroded samples were mounted (without cleaning) in thermosetting resin and metallographically polished. Images, EDS and elemental mapping analyses were obtained from a LEO 1450VP Microscope coupled with energy dispersive X-ray analyzer (EDAX). Also, the corrosion products found after cleaning the exposed samples from EIS were analyzed by the X-ray diffraction technique (XRD), utilizing a diffractometer operating with Cu K $\alpha$  radiation, and results were interpreted utilizing the Powder Diffraction Data File [18].

## 3. RESULTS AND DISCUSSION.

### 3.1 Corrosion Physical Characterization.

Figure 1 shows two micrographs of Inconel-600 exposed to the high sulfate (a), and high vanadium molten salts (b) at 700°C for 120 h of exposure. The image of the sample exposed to the high sulfate mixture presented an intergranular corrosion process over the whole surface, in which the grain boundaries are clearly observed. The shape of the grains is irregular, and their size is in the range of 15  $\mu\text{m}$  to 100  $\mu\text{m}$ .

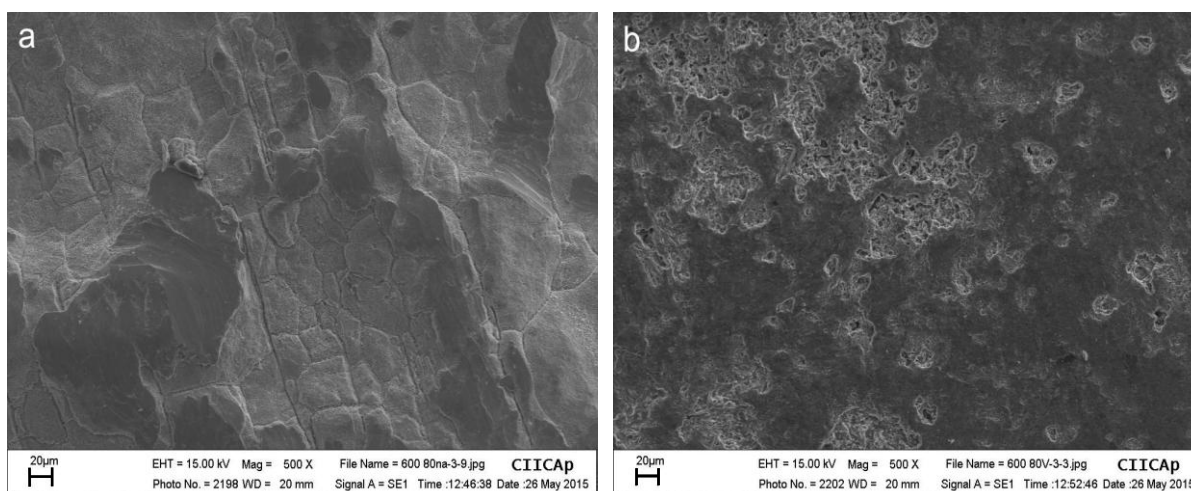


**Figure 1.** Images of Inconel-600 after exposure in a) high sulfate molten salt and b) high vanadium molten salt for 120 h at 700 °C.

The exposed sample to high vanadium molten salt showed a generalized corrosion process, observing the presence of localized attacks through the whole surface. The image of the corroded

sample shows a more general dissolution of the surface showing cavities and pores, which were probably generated by selective chemical dissolution, which led to a consequent mass loss. When corrosion phenomenon produces pores, these facilitate the penetration of corrosive species and the oxygen diffusion is carried out through the pores. Such as said before, the porosity indicates the presence of selective dissolution of some alloying elements of the material; nevertheless, if the protective corrosion products layer is passive, the diffusion of oxygen and some corrosive species can be avoided [19].

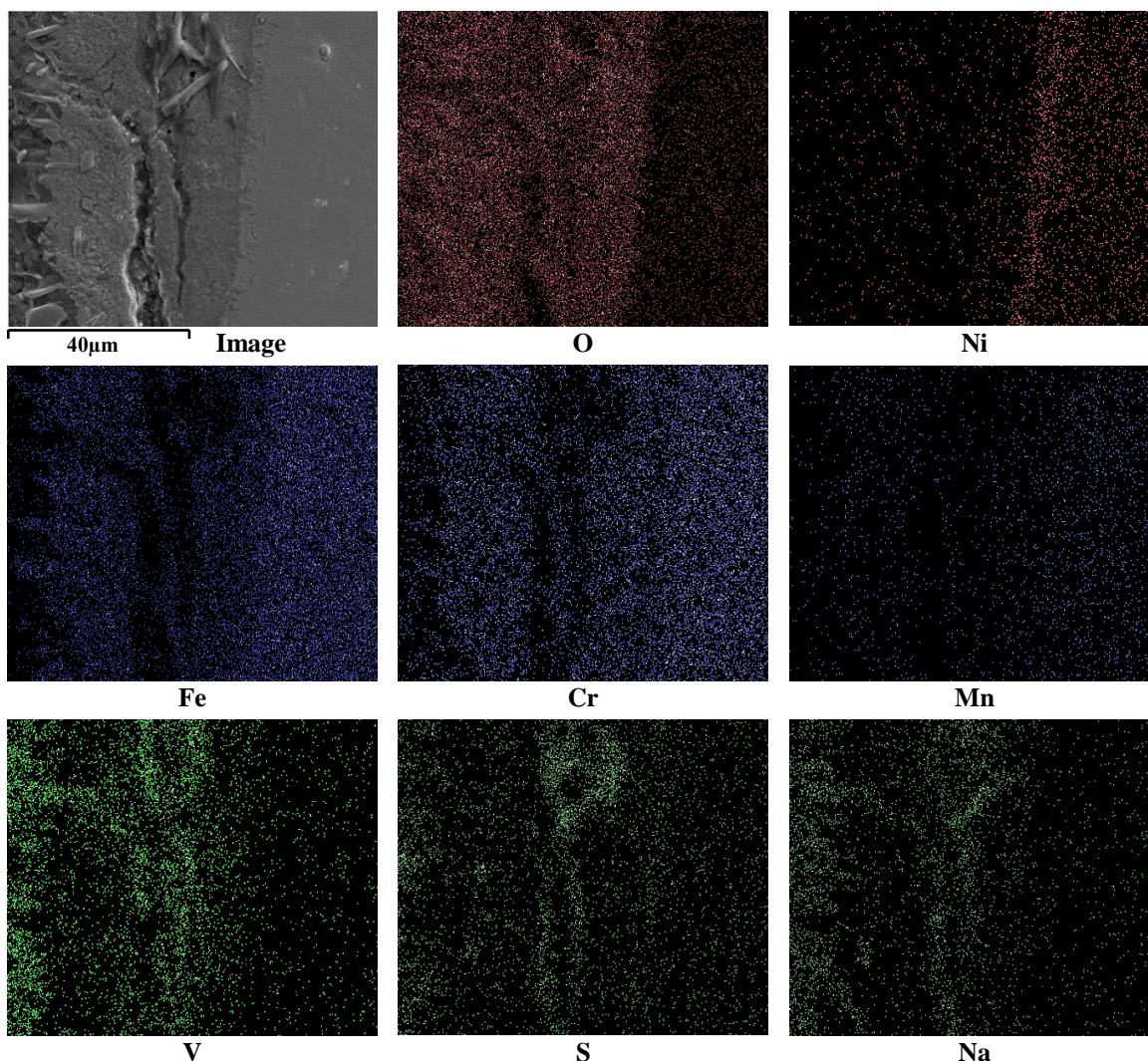


**Figure 2.** Electron image of the metal-scale interface and X-ray mappings of O, Ni, Fe, Cr, Mn, V, S and Na of Inconel-600 after exposing 120 h to high sulfate molten salt at 700°C.

Figure 2 shows cross section and X-ray maps of O, Ni, Fe, Cr, Mn, V, S and Na of Inconel-600 after exposing 120 h to high sulfate molten salt at 700°C. A combined layer of O, Fe, Cr and V as corrosion products was observed coexisting in the same place, far away of the metal-corrosion products interface, being evident the dissolution of Cr and Fe. Therefore, the formation of oxides and metal vanadates compounds can be assumed. In the corrosion products/metal interface, Cr depletion is

observed. Chromium oxide is one of the most protective compounds when the molten salts of sodium sulfate and vanadium pentoxide are present [20-22]. It is possible that chromium oxide formed at the beginning of the exposure as a protective layer started to dissolve by the effect of the oxidant species of the molten salt, since Cr mapping presents a discontinuous and non-coherent layer over the metallic surface and far away from the metal/corrosion products scale. The Ni mapping shows a dense layer inside the matrix of the metal, which was possibly due to the depletion of the chromium. The sulfur mapping shows a low concentration of this compound at the corrosion products-metal interface. The presence of sulfur can be related to the presence of chromium sulphides. The metal sulphides can be oxidized when reacting with the available oxygen, therefore the release of sulfur is possible. This mechanism has been called oxidation/sulfidation, and it has been previously proposed by Spengler [23]. However, according to the sulfur mapping, sulfur is part of the scale over the surface, and there was no evidence of diffusion to the matrix of the alloy, therefore and according to the oxygen mapping, an oxidation corrosion process through the grain boundaries could be the type of corrosion suffered by the Inconel-600 exposed to the high sulfate molten salt. Studies have indicated that Ni forms a moderately stable oxide; however,  $\text{Cr}_2\text{O}_3$  is an even more stable oxide [24]. In this case, it is possible that NiO played an important role once  $\text{Cr}_2\text{O}_3$  dissolved in time, nevertheless, Inconel-600 suffered an intergranular corrosion process due to oxidation, such as shown in the oxygen mapping, where a  $5\mu\text{m}$  oxygen layer is inside the matrix of the metal. On the other hand, it is also possible that the high Ni content (72%) of the Inconel-600 helps to decrease the corrosion rate [25].

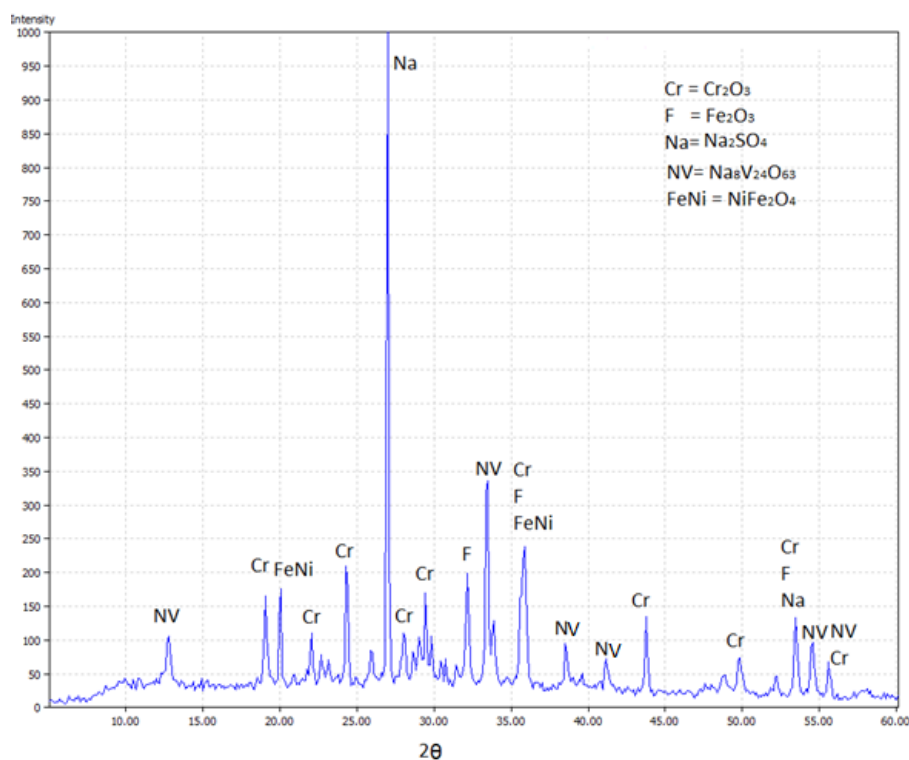


**Figure 3.** X-ray diffraction results of corrosion products of Inconel-600 exposed to the high sulfate molten salt for 16 h at 700 °C.

Figure 3 shows the XRD analysis results of the corrosion products obtained from the exposure of Inconel-600 to the high sulfate molten salt at 700°C. The spectrum shows that during the corrosion process  $\text{Cr}_2\text{O}_3$ ,  $\text{Fe}_2\text{O}_3$  and the spinel  $\text{NiFe}_2\text{O}_4$  were formed, NiO oxide was not identified, which is according to the Ni mapping. On the other hand, a sodium vanadyl vanadate ( $\text{Na}_8\text{V}_{24}\text{O}_{64}$ ) was formed, which can be present when a sulfate-vanadate mixture melts at high temperatures. Also, unreacted  $\text{Na}_2\text{SO}_4$  was found.

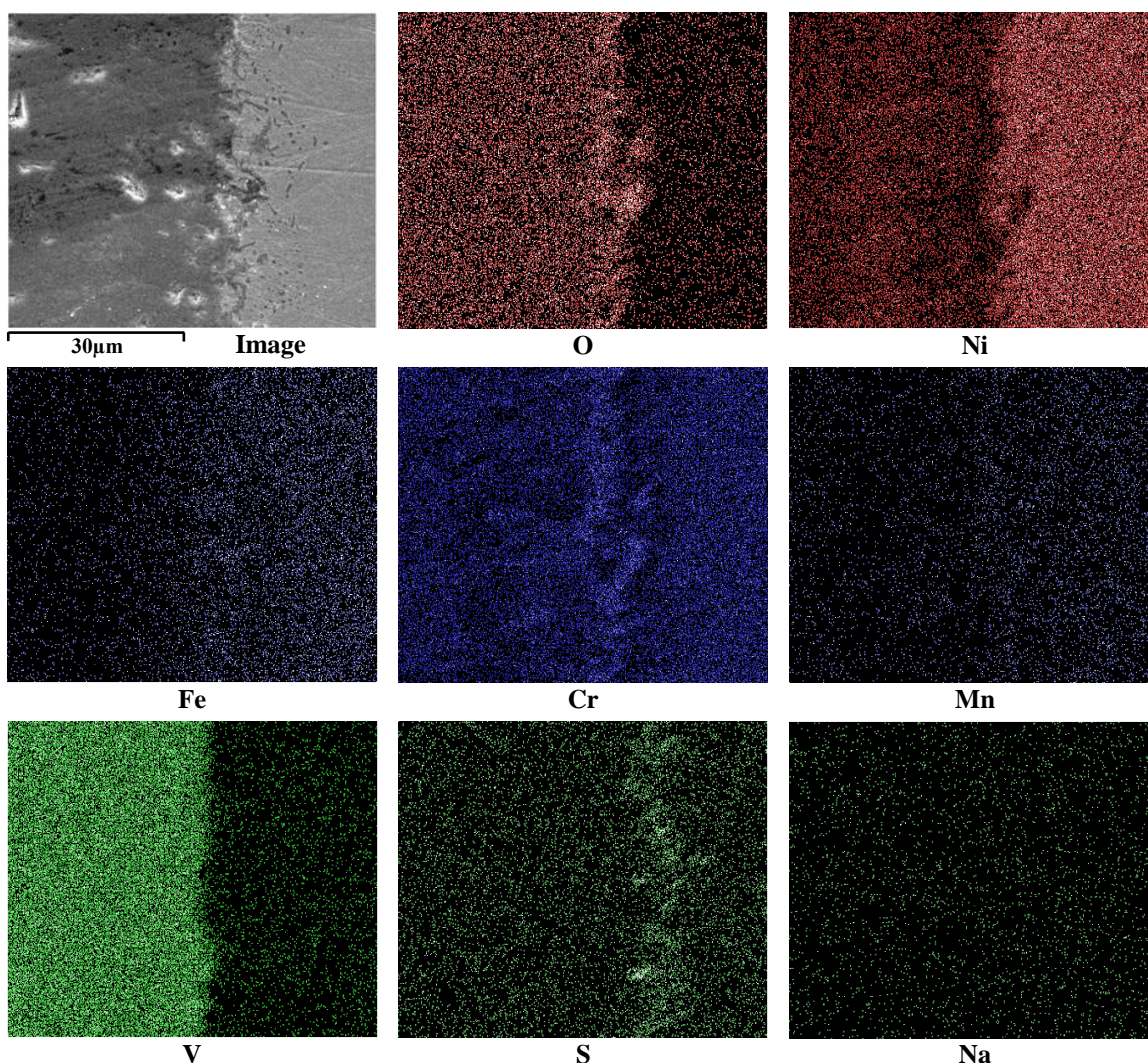


**Figure 4.** Electron image of the metal-scale interface and X-ray mappings of O, Ni, Fe, Cr, Mn, V, S and Na of Inconel-600 after exposing 120 h to high vanadium molten salt at 700°C.

Figure 4 shows a cross section and X-ray mappings of O, Ni, Fe, Cr, Mn, V, S and Na of Inconel-600 after exposing 120 h to high vanadium molten salt at 700°C. According to the elemental mapping analysis, a layer rich in O, Ni, Cr and V was observed far away the scale over the surface, such layer may be constituted by NiO and  $\text{Cr}_2\text{O}_3$  dissolved especially by the effect of vanadium species. It is noted that in the case of the exposure to high sulfate molten salt,  $\text{Fe}_2\text{O}_3$  and  $\text{Cr}_2\text{O}_3$  were

dissolved; on the contrary, during the exposure to high vanadium molten salt, the dissolution of NiO and  $\text{Cr}_2\text{O}_3$  was carried out. The presence of Cr, Ni, O and V far away the scale confirms the synergistic dissolution of Cr and Ni [26-27], possibly as metallic vanadates. Also, Cr and O mappings shows a discontinuous and not so dense layer just over surface, evidencing that it was possible the formation of a protective  $\text{Cr}_2\text{O}_3$  layer at the beginning of the exposure to the high vanadium molten salt. Cr oxidation resulted in an area depleted in Cr inside the alloy; such depleted area has been occupied by nickel [28]. It seems that due to the discontinuous chromium oxide, the diffusion of sulfur into the matrix of the alloy was evident. Observing the S and Ni mappings, it is possible to state the formation of nickel sulphides into the matrix, just 10  $\mu\text{m}$  below the surface. The diffusion of sulfur inside the alloy is a typical phenomenon of continuous dissolution of the protective oxides [29,30]. From the O and Ni mappings, a NiO layer was formed and dissolved, nevertheless, it is possible that a thin NiO layer keeps just in the corrosion products/metal scale, but due to the diffusion of certain amount of sulfur inside the metal, this NiO layer is not expected to be so protective and coherent.

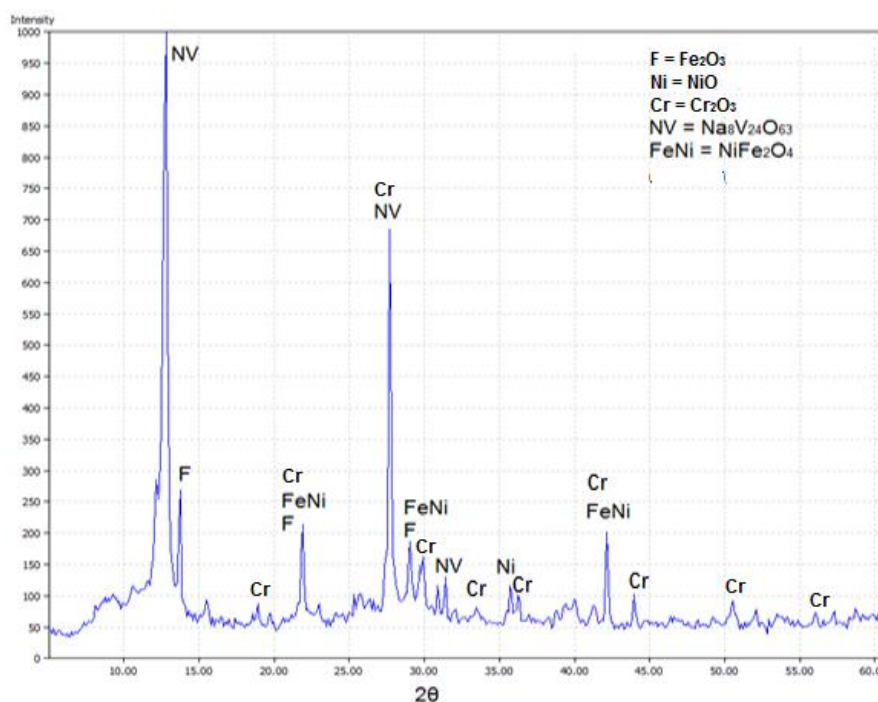


**Figure 5.** X-ray diffraction results of corrosion products of Inconel-600 exposed to the high vanadium molten salt for 120 h at 700 °C.

Figure 5 presents the XRD pattern of the corrosion products obtained from the exposure of Inconel-600 to the high vanadium molten salt at 700°C, which confirms the presence of  $\text{Fe}_2\text{O}_3$ ,  $\text{Cr}_2\text{O}_3$  and NiO. The presence of sodium vanadyl vanadate ( $\text{Na}_8\text{V}_{24}\text{O}_{63}$ ) and the spinel ( $\text{NiFe}_2\text{O}_4$ ) peaks were also detected.

### 3.2 Electrochemical Measurements.

#### 3.2.1 Potentiodynamic Polarization Curves.

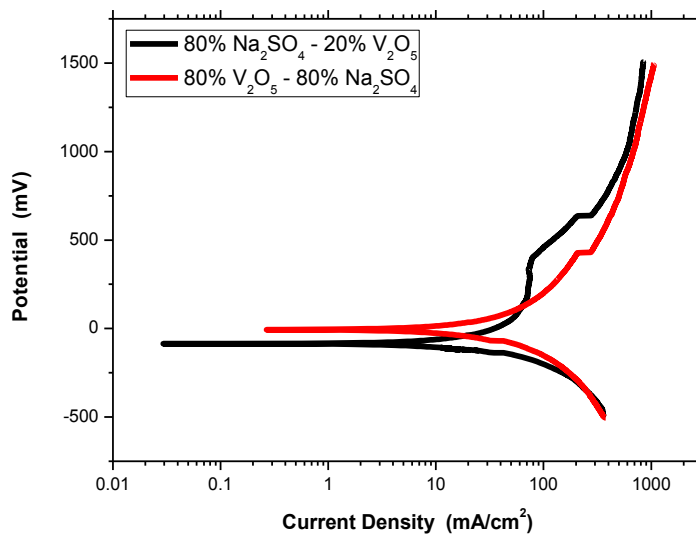


**Figure 6.** Polarization curves for Inconel-600 exposed to high sulfate and high vanadium molten salts at 700 °C.

Figure 6 shows the potentiodynamic polarization curves for Inconel-600 exposed to high sulfate and high vanadium molten salts at 700 °C. In both corrosive systems, Inconel-600 presents an active behavior; therefore, the corrosion products formed on the Inconel-600 are expected to be susceptible to dissolution, which would provide only partial protection [31]. These results are in accordance with the results of the physical characterization of the corroded samples. The Inconel-600 exposed to the high sulfate molten salt presented a corrosion potential  $E_{\text{corr}}$  of -85.2 mV, whereas that obtained for the exposure in the high vanadium molten salt of -6.85 mV (nobler). On the other hand, the corrosion current density ( $i_{\text{corr}}$ ) obtained by the Tafel extrapolation method showed very similar values in both corrosive systems, being the value obtained from the exposure in the high sulfate molten salt of 17.168 mA/cm<sup>2</sup>; whereas that obtained from the exposure in the high vanadium molten salt of 18.165 mA/cm<sup>2</sup>. According to the polarization curves, the Inconel-600 seems to have similar corrosion rates, even though, it is important to note that thermodynamically speaking, Inconel-600 behaves nobler when exposing to the high vanadium molten salt. This nobler behavior can be confirmed through the morphological characterization, since the type of corrosion suffered by Inconel-600 exposed to the high vanadium molten salt was a generalized corrosion, accompanied with cavities and pores; whereas that observed in the exposure to the high sulfate molten salt was an intergranular corrosion process, which is expected to be more destructive for the metallic materials.

It is important to mention that the potentiodynamic polarization curves indicate short-term behavior (when the corrosive system just achieves the steady state), and this fact may change under long-term exposures as a result of some chemical changes in the composition of the molten salt due to the dissolution reactions and the formation of secondary corrosion products.

**Table 2.** Electrochemical parameters of potentiodynamic polarization curves of the Inconel-600 exposed to the high sulfate and high vanadium molten salt at 700°C.

Molten Salts	$\beta_a$ (mV/dec)	$\beta_c$ (mV/dec)	$i_{corr}$ (mA/cm <sup>2</sup> )	$E_{corr}$ (mV)
80% mol Na <sub>2</sub> SO <sub>4</sub> – 20% V <sub>2</sub> O <sub>5</sub>	128.15	73.297	17.168	-85.2
80% mol V <sub>2</sub> O <sub>5</sub> – 20% Na <sub>2</sub> SO <sub>4</sub>	153.43	114.94	18.165	-6.8584

With respect to the Tafel slopes  $\beta_a$  and  $\beta_c$ , it is possible to say that values between 100-120 mV/dec represent a typical activation controlled system [32], so that, in this particular case, it is possible to state that the corrosive process was not controlled purely by activation or diffusion, a mixed corrosion controlled system may exist.

3.2.2 Electrochemical Impedance Spectroscopy.

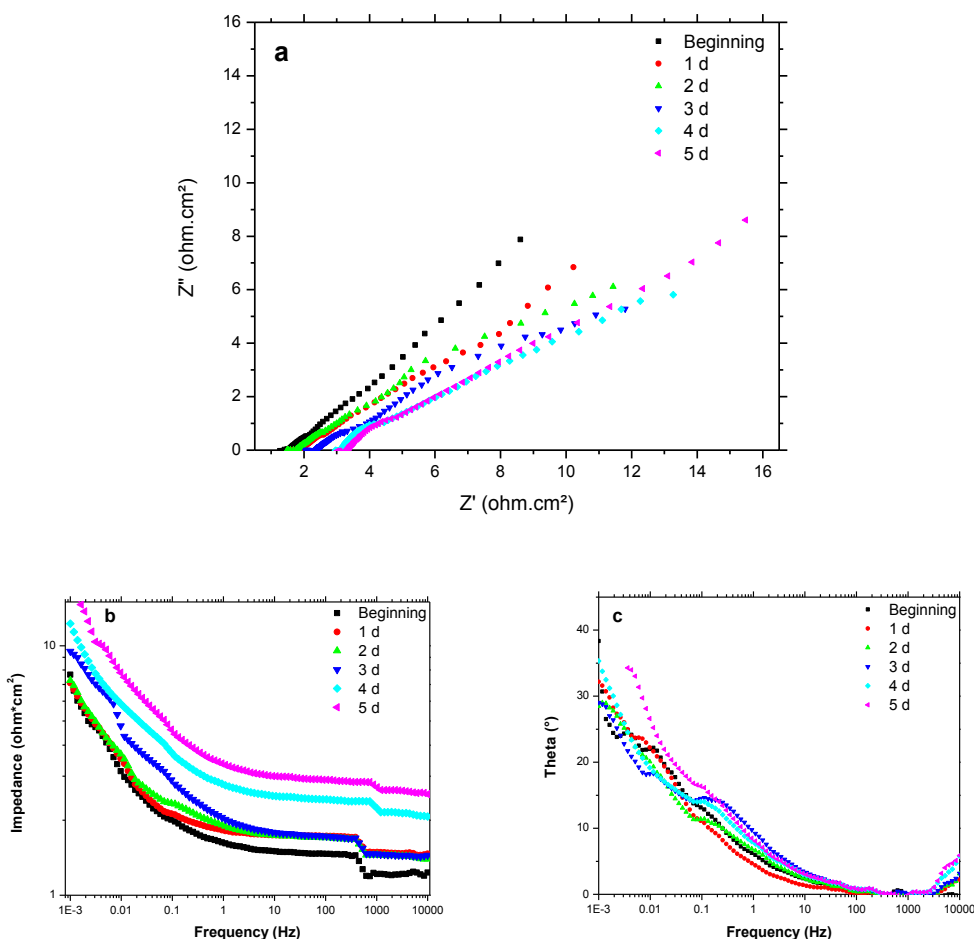


**Figure 7.** Nyquist (a) and Bode diagrams ((b) Impedance and (c) phase) of Inconel-600 obtained from the exposure to the high sulfate molten salt at 700 °C.

Figure 7 shows the Nyquist and Bode diagrams for the Inconel-600 after being exposed to the high sulfate molten salt for 120 h at 700 °C. It can be observed that initially the material exhibits a mixed corrosion behavior: at high frequency, the corrosion process is controlled by charge transfer and at low frequencies by mass diffusion (45° line). The presence of a semicircle indicates the presence of a single oxide layer formed over the metallic surface at the beginning of the corrosion process [33]. According to the physical characterization and XRD results, this oxide layer was Cr<sub>2</sub>O<sub>3</sub>, which is expected to be compact and adherent. The diffusion of species could be either, from the metal surface as metallic ions to the scale, or from the molten salts as vanadium, oxygen and sulfur species to the metal surface. At the second day, the results show a charge transfer controlled process, since the Nyquist diagram shows a first semicircle at high frequencies, and a second semicircle at low frequencies. However, due to the selected frequency range (0.001-10000 Hz), the second semicircle may not be completely formed, however the phase angle diagram (Fig. 7.c) shows clearer the tendency in the formation of the second semicircle.

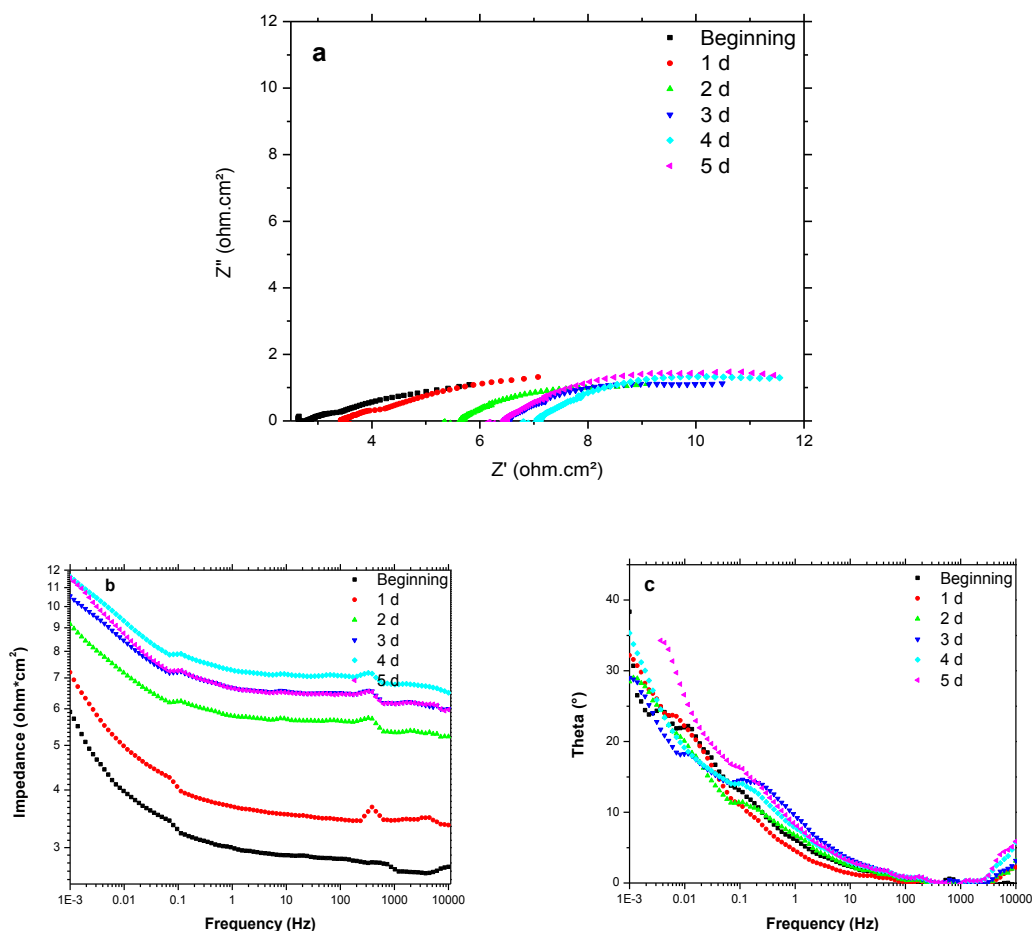


**Figure 8.** Nyquist (a) and Bode diagrams ((b) Impedance and (c) phase) of Inconel-600 obtained from the exposure to the high vanadium molten salt at 700 °C.

This behavior can be a characteristic of materials forming a protective layer on the surface. SEM analyses showed two oxide layers, one of  $\text{Cr}_2\text{O}_3$  and another one of  $\text{Fe}_2\text{O}_3$ , indicating that the material presented certain resistance to be corroded. This fact indicates that at the beginning of the exposure, Inconel-600 probably formed a protective layer, which suffered some dissolution after 24 h becoming in a porous layer. After 48h, the porous layer passivated and the charge-transfer resistance ( $R_{ct}$ ) increases, such as it can be seen with the increase of the diameter of the semicircle. From the impedance Bode diagram (7.b), the charge-transfer resistance is almost constant until the second day, after that,  $R_{ct}$  increases until the end of the experiment. The increase in  $R_{ct}$  must be due to the presence of the NiO layer formed below the  $\text{Cr}_2\text{O}_3$ , such as it was said in the physical characterization section.

Figure 8 shows the Nyquist and Bode diagrams for the Inconel-600 exposed to the high vanadium molten salt at 700 °C for 120 h. A charge-transfer controlled process can be observed from the beginning until the end of the experiment. From the Nyquist diagram two semicircles are observed, which present an increase in diameter from the beginning to the fourth day. The increase of the diameter of the semicircles means an increase of the charge transfer resistance ( $R_{ct}$ ). When  $R_{ct}$  increases the corrosion rate decreases, and a protective and passive oxide layer is present, on the other hand, when  $R_{ct}$  diminishes, the corrosion rate increases, which is due to the dissolution of the protective layer due to the effect of the corrosive molten salt species [34,35]. In this corrosive system, in which the high vanadium molten salt is more acidic and therefore more corrosive [36], the  $\text{Cr}_2\text{O}_3$  layer formed initially on the surface had a presumably protective behavior. According to EIS results, especially from the Bode impedance diagram (8.b), at the fifth day,  $R_{ct}$  was basically the same than that of the fourth day, therefore, this protective layer might be partially dissolved, such as it was confirmed by the Cr mapping from SEM analyses. Also, the presence of a thin NiO layer as demonstrated from the corresponding mapping could be the reason for which  $R_{ct}$  increases.

#### 4. CONCLUSIONS

The corrosion performance of the Inconel-600 exposed to the high sulfate molten salt and the high vanadium molten salt at 700 °C during 120 h was determined using two electrochemical techniques. According to the results, it is possible to state the next conclusions:

Inconel-600 showed a different corrosion mechanism after exposing to both molten salts. From SEM results, Inconel-600 suffered a generalized corrosion process by sulfidation when it was exposed to the high vanadium mixture, since the initially formed chromium oxide was become into a porous layer, so that, sulfur diffused into the matrix of the metal, probably forming nickel sulphides. On the other hand, Inconel-600 exposed to the high sulfate molten salt presented an intergranular-oxidation process, so that, even though it seems that  $\text{Cr}_2\text{O}_3$  was more adherent and stable, also suffered a dissolution process. EIS results showed a charge transfer controlling process when Inconel-600 was exposed to the high vanadium molten salt, and a mixed corrosion controlling mechanism (charge transfer and diffusion) when it was exposed to the high sulfate molten salt. EIS results were in

congruence with the physical characterization obtained by SEM. The polarization curves indicated that both cases were active systems, corroding at a similar corrosion rate.

## References

1. K. D. Gupta and R. A. Rapp, *J. Electrochem. Soc.*, 127-10 (1980) 2194.
2. Y. Harada, S. Naito, T. Tsuchiya and Y. Nakajima, *Mitsubishi tech. bull.*, (1981) 85.
3. W. D. Halstead, *J. Inst. Fuel*, 45 (1970) 234.
4. A.W. Moreno, R. I. Salgado and L. Martinez, Molten salt corrosion of heat resisting alloys, *CORROSION/95 NACE International*, Orlando FL, USA (1995) 465.
5. T. S. Sidhu, S. Prakash and R. D. Agrawal, *Curr. Sci.*, 90-1 (2006) 41.
6. E. Otero, A. Pardo, F. J. Perez, J. F. Alvarez and M. V. Utrilla, *Corros. Sci.*, 39-1 (1997) 133.
7. A. W. Moreno, Y. M. Martinez and L. Martinez, High temperature corrosion enhanced by residual fuel oil ash deposits, *CORROSION/94 NACE International*, Baltimore MD, USA (1994) 185.
8. A. J. Cutler, W. D. Halstead, A. B. Hart, J. W. Laxton and C. G. Stevens, An approach to the mechanism of the corrosion of steels in oil-fired boilers, Central Electricity Research Laboratories, Report RD/L/N 194/70, (1970) Surrey, U.K.
9. T. S. Sidhu, R. D. Agrawal and S. Prakash, *Surf. Coat. Technol.*, 198 (2005) 441.
10. J. D. Matthew and J. D. Stephen, *Superalloys: A Technical Guide*, The Materials Information Society, ASM International, (2002) Ohio, USA
11. S. Kalpakjian and S. R. Schmid, *Manufacturing, Engineering and Technology*, Prentice Hall Inc., (2001) New Jersey, USA.
12. G. Gao, F. H. Stott, J. L. Dawson and D. M. Farrell, *Oxid. Met.*, 33 (1990) 79.
13. D. M. Farrell, W. M. Cox, J. L. Dawson and P. D. Bottomley, Electrochemical interfaces in high temperature sulphidation and oxidation reactions, *CORROSION/89 NACE International*, New Orleans LA, USA (1989) 2.
14. D. M. Farrell and F. H. Stott, Electrochemical Aspects of High Temperature Corrosion Reactions in Combustion Systems, *European Federation of Corrosion*, Manchester, U.K. (1991) 122.
15. C. Cuevas Arteaga, *Corros. Sci.* 50 (2008) 650.
16. Y. Harada and T. Kawamura, *Mitsubishi Tech. Bul.*, 139 (1980).
17. H. J. Ratzer, Electrochemical studies of uncoated and coated Ni-base super alloys in molten sulphate, *4th International Symposium on high temperature corrosion and protection of materials*, Les Embiez, France (1996) 1-8.
18. L.G. Berry (Ed.), *Powder Diffraction Data File – Inorganic Phases*, Publication of the Joint Committee on Powder Diffraction Standards, International Center for Diffraction Data, Swarthmore PA, USA (1980).
19. Y. T. Zhao, S. W. Yang, C. J. Shang, X. M. Wang, W. Liu and X. L. He, *Mat. Sci. Eng., A*, 454 (2007) 695.
20. J. Tuominen, M. Honkanen, M. Usitalo, S. Ahmaniemi, P. Vuoristo and T. Mäntylä, Hot corrosion resistant laser coatings in diesel engine, Laser Application Laboratory, Institute of Materials Science, Tampere University of Technology, Report No. 19, (1985) Tampere, Finland.
21. C. Cuevas Arteaga, J. Uruchurtu Chavarin, J. Porcayo-Calderon, G. Izquierdo Montalvo and J. González, *Corros. Sci.*, 46 (2004) 2663.
22. W. C. Xiang, A. Nishikata and T. Tsuru, *High Temperature Corrosion of Advanced Materials and Protective Coating*, Elsevier Science Publishers, (1992) North Holland.
23. C. J. Spengler and R. Viswanthan, *Metall. Trans.*, 3 (1972) 161.
24. N. Birks, G. H. Meier and S. F. Pettit, *Introduction to the high temperature oxidation of metals*, Cambridge University Press, (2006) Cambridge, U.K.
25. S. H. Cho, J. M. Hur, C. S. Seo, J. S. Yoon and S. W. Park, *J. Alloys Compd.*, 468 (2009) 263.

26. Y. L. Nava, Y. S. Zhang, M. Takemoto and R. A. Rapp, *Corrosion*, 52 (1996) 680.
27. Y. S. Hwang and R. A. Rapp, *Corrosion*, 45 (1989) 933.
28. J. G. Gonzales, A. L. Ramirez, M. Salazar, J. C. Porcayo, G. Rosas and A. M. Villafaña, *Mater. Sci. Eng., A* 399 (2005) 344.
29. G. M. Lu, S. Z. Shang, J. J. Yu and J. G. Yu, *Appl. Mech. Mater.*, 52 (2011) 1538.
30. G. S. Solano, J. C. Porcayo, J. G. Gonzalez, V. M. Salinas, J. A. Ascencio and L. M. Gomez, *Adv. Mater. Sci. Eng.*, (2014) 8.
31. C. Cuevas Arteaga, J. Uruchurtu Chavarin, J. González, G. Izquierdo Montalvo, J. Porcayo-Calderon and U. Cano-Castillo, *Corros. Sci.*, 60 (2004) 548.
32. W. Skinner, *Br. Corros. J.*, 22-3 (1987) 172.
33. J. L. Trinstancho, M.S. Carrillo and R. S. Jabalera, *Int. J. Electrochem. Sci.*, 6/2 (2011) 419.
34. X. Zheng, R. A Rapp, *J. Electrochem. Soc.*, 142 (1995) 142.
35. W. Y. Mei and R. A Rapp, *J. Electrochem. Soc.*, 138 (1991) 2683.
36. C. L. Zheng, W. Wang and W. T. Wu, *Oxid. Met.*, 53-3 (2000) 289.

© 2017 The Authors. Published by ESG ([www.electrochemsci.org](http://www.electrochemsci.org)). This article is an open access article distributed under the terms and conditions of the Creative Commons Attribution license (<http://creativecommons.org/licenses/by/4.0/>).